Photon-Counting Detectors in Computed Tomography: Physics, Detector Architectures, Signal Formation, and Clinical Translation — A Systematic Review

Manpreet Singh[1], Pallavi Saini[2]
[1]*Junior Technologist, PGIMER, Chandigarh*
[2] *Junior Technologist, PGIMER, Chandigarh*

Background: Photon-counting detector computed tomography (PCD-CT) represents a fundamental detector-level transformation in diagnostic X-ray imaging, shifting the paradigm from energy-integrating detectors (EIDs) to direct-conversion, energy-resolving semiconductor sensors.

Methods: A systematic literature synthesis was conducted across primary physics primers, preclinical prototype evaluations, and clinical trial literature from major databases (PubMed/MEDLINE, IEEE Xplore, Web of Science, and Google Scholar) covering semiconductor sensor physics, front-end application specific integrated circuit (ASIC) design, signal formation dynamics, and reconstructive outputs.

Results: PCD-CT replaces the indirect two-step conversion of scintillators with direct electron-hole pair generation in high-atomic-number semiconductor crystals (cadmium telluride [CdTe], cadmium zinc telluride [CZT]) or edge-on silicon (Si). Absorbed X-ray energy E_dep generates femtocoulomb-scale charge packets that drift under high bias voltage (800-1000 V) to pixelated anodes. Small-pixel geometries (p/d < 0.2) exploit weighting potential localization to produce fast, electron-dominated induced current pulses. Front-end pulse shaping and comparator logic classify incoming pulses into multiple energy bins while setting the lowest threshold (T_0 20-25 keV) above the electronic noise floor, completely eliminating classical electronic noise. Physical non idealities—including charge sharing, K-shell fluorescence escape (26.7 keV for Cd, 31.8 keV for Te), and pulse pileup at clinical flux (> 10^9 photons/s/mm^2)—distort the Spectral Response Function and require hardware charge-summing circuits and anti-coincidence logic.

Discussion: Clinical deployment of PCD-CT yields spatial resolution up to 16-17 lp/cm (0.3 mm detail), radiation dose reductions of up to 80-85%, and intrinsic multi-threshold spectral imaging (Virtual Monoenergetic Imaging, iodine density quantification, Z_{eff} mapping, and K-edge decomposition) from every acquisition. Continued advancement in ASIC throughput, polarization suppression, and deep learning spectral reconstruction will solidify PCD-CT as the standard for diagnostic radiology.

Keywords: Photon-counting CT, Semiconductor detectors, Cadmium telluride, Pulse pileup, Charge sharing, Virtual monoenergetic imaging, Material decomposition, K-edge imaging

INTRODUCTION

For over five decades, clinical computed tomography (CT) has relied almost exclusively on energy integrating detector (EID) technology. In an EID system, post-patient X-ray photons interact with a solid state scintillating crystal, such as gadolinium oxysulfide (GOS) or gadolinium oxide[1,3]. This interaction converts X-ray energy into visible light photons, which subsequently travel to an attached photodiode array to generate an analog electrical current[1]. The front-end electronics integrate this accumulated charge over a finite measurement window (projection reading).

While EID systems have achieved high gantry rotation speeds and wide anatomical coverage, two fundamental physical constraints restrict their ultimate diagnostic capabilities:

1. Scintillation Spread and Septal Dead Zones: Optical light generated within the scintillator spreads isotropically in all directions. To prevent severe optical crosstalk between adjacent detector pixels, reflective septa (optically opaque layers, typically TiO2-based) must be interspaced between individual scintillator cells. These septa create physical "dead zones" of approximately 0.1-0.2 mm width. As pixel pitch is reduced below 0.8 mm to improve spatial resolution, the relative fraction of inactive septal area increases dramatically, causing severe geometric dose inefficiency where up to 20-30% of post-patient radiation is wasted[1,4].

2. Energy Weighting and Electronic Noise Penalty: Because EIDs integrate total deposited energy, the generated detector signal S follows a linear energy-weighting relationship:

$$S = \int_0^{E_{\max}} D(E)\, N(E)\, dE \approx \int_0^{E_{\max}} E\, N(E)\, dE$$

where D(E) is the energy-dependent detector responsivity, N(E) is the absorbed photon flux, and E_max is the maximum tube voltage[1,2]. Consequently, high-energy photons—which carry lower soft-tissue and contrast-agent attenuation information—contribute disproportionately to the signal, whereas low-energy photons near the K-edge of iodine (33.2 keV) are downweighted. Furthermore, at low photon flux (such as in large patients, thick anatomical regions, or ultra-low-dose screening protocols), low-amplitude electronic noise from the photodiodes and preamplifiers exceeds Poisson quantum noise, introducing severe noise streaks, dark-current drift, and Hounsfield Unit (HU) instabilities[1,8].

Photon-counting detector computed tomography (PCD-CT) fundamentally overcomes these barriers by replacing indirect scintillators with direct-conversion semiconductor materials. When an X-ray photon interacts with a PCD sensor crystal, it generates electron-hole pairs directly without an intermediate light phase[6,7]. An applied high-voltage electric field drifts these charges to micro-pixelated anodes, inducing short current pulses (10 ns) that are amplified, shaped, and evaluated event-by-event by fast application-specific integrated circuits (ASICs)[7,8].

By comparing peak pulse heights against preset energy thresholds, PCD-CT achieves three revolutionary diagnostic advantages:

- Complete Rejection of Electronic Noise: Setting the primary threshold T_0 above the baseline electronic noise floor eliminates thermal and amplifier noise from registered counts[1,8].
- Ultra-High Spatial Resolution Without Dose Penalties: Direct conversion avoids light spread, eliminating the need for optical septa. Detector pixel dimensions can be reduced to 0.1--0.3 mm while preserving active geometric fill factor[4,10].
- Intrinsic Energy-Resolved (Spectral) Imaging: Simultaneous evaluation across multiple energy thresholds sorts incoming photons into distinct energy bins from a single tube exposure, enabling quantitative material decomposition, virtual monoenergetic imaging, and K-edge detection[2,6].

METHODS

Literature Search Strategy and Ingestion

A systematic narrative literature review was conducted to evaluate the technical, physical, and clinical literature regarding photon-counting detector CT[3,4,6]. Academic databases including PubMed/MEDLINE, IEEE Xplore, Web of Science, Scopus, and Google Scholar were searched for peer-reviewed journal articles, conference proceedings, and foundational physics primers published through 2026[3,7].

Search queries combined domain keywords using Boolean operators:

("photon-counting CT" OR "photon-counting detector" OR "PCD-CT")

- AND ("direct conversion" OR "CdTe" OR "CZT" OR "silicon detector" OR "charge
- sharing" OR "pulse pileup" OR "weighting potential") AND ("virtual monoenergetic

imaging" OR "material decomposition" OR "K-edge" OR

- "radiation dose efficiency" OR "IMRAD review")

Inclusion and Exclusion Criteria

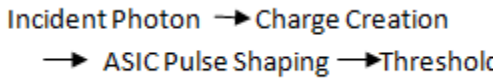
Studies were included if they investigated:

1. Fundamental semiconductor physics and charge-carrier transport dynamics in PCD sensors.
2. Front-end ASIC signal shaping, baseline restoration, and multi-threshold comparator logic.
3. Physical non-idealities, including charge sharing, K-shell fluorescence escape, polarization, and pulse pileup modeling.
4. Quantitative reconstructive performance, spatial resolution (MTF), noise-power spectrum (NPS), detective quantum efficiency (DQE), and clinical task evaluations on commercial or prototype PCD CT systems (including Siemens NAEOTOM Alpha, GE Photonova Spectra, Canon/Redlen CZT, and prototype deep-silicon platforms)[5,10,12].

Articles focusing exclusively on industrial non-destructive testing, nuclear medicine gamma cameras, or non-CT single-photon counting applications were excluded.

Synthesis Methodology: The Causal Signal Chain

To synthesize findings rigorously, retrieved data were organized along an end-to-end causal measurement chain[7,9]:



Every physical mechanism, electronic transformation, and clinical output was analyzed with respect to its exact position along this causal sequence to explain how low-level detector non-idealities propagate into final reconstructed CT images.

Results

Physics of Direct Conversion and Charge Creation

In direct-conversion PCDs, the post-patient polychromatic X-ray beam enters a semiconductor crystal subjected to a strong reverse bias voltage (approx 800--1000 V). X-ray photons undergo photoelectric absorption or Compton scattering, transferring energy E_{dep} to bound atomic electrons.

The primary photoelectron or recoil electron rapidly creates a cascade of secondary ionization events, generating mobile electron-hole pairs[7,10].

The mean number of electron-hole pairs ($\bar{N}_{eh}$) generated by a deposited energy E_{dep} is governed by the semiconductor's ionization energy Ei:

$$\bar{N}_{eh} = \frac{Edep}{Ei}$$

The effective ionization energy Ei is substantially larger than the bandgap energy Eg because a

portion of the absorbed energy is dissipated via optical and acoustic phonon lattice vibrations. The unweighted initial charge yield Q_0 delivered to the front-end amplifier is:

$$Q_0 = e.\frac{Edep}{Ei}$$

where e = 1.602 $x10^{-19}$ C is the elementary charge.

As detailed in Table 1, for a typical diagnostic X-ray photon with Edep = 60 keV, a semiconductor sensor generates an initial charge packet Q_0 on the order of 2.0-2.7 femtocoulombs (1.3 x 10^4-1.7 x 10^4 electrons).

Physical & Electronic Property	Cadmium Telluride (CdTe)	Cadmium Zinc Telluride (CZT)	Silicon (Si)	Gadolinium Oxysulfide (GOSEID)

Detection Mechanism	Direct Semiconductor	Direct Semiconductor	Direct Semiconductor	Indirect Semiconductor
Atomic No (Z)	48,52	48, 30, 52	14	64, 16, 8
Density (g/cm^3)	5.85	5.78	2.33	7.32
Bandgap E_g (eV) at 300 K	1.44	1.57	1.12	N/A (Scintillator)
Mean Ionization Energy E_i (eV)	4.43	4.63	3.60	Approx 20 eV/photon
Charge Yield $\bar{N}_{eh}$ at 60 keV	13,540 e-h pairs	12,960 e-h pairs	16,670 e-h pairs	Approx 1200 e (photodiode)
Intial Charge Packets Q_0 at 60 keV	2.17 fC	2.08 fC	2.67 fC	N/A (Integrated)
Electron Mobility μ_e (cm^2/V.s)	1000-1100	1000-1200	1450	N/A
Hole Mobility μ_h (cm^2/V.s)	50-80	50-80	450	N/A
Typical Sensor Thickness (d)	1.4-2.0 mm	1.4-2.0 mm	30mm (edge on)	1.0 mm
K-edge Energies (keV)	Cd: 26.7, Te: 31.8	Cd: 26.7, Te: 31.8	Si: 1.84 (Negligible)	Gd: 50.2

Due to the stochastic nature of secondary ionization cascades, carrier generation exhibits subPoissonian fluctuations quantified by the Fano factor F ≈0.1-0.15. The theoretical variance in generated carrier count is: $\sigma^2_N = F.\bar{N}$ establishing an intrinsic physical limit on energy resolution before transport and electronic noise enter the chain.

Sensor Materials, Transport Dynamics, and the Small-Pixel Effect

Material Selection: High-Z Semiconductors vs. Deep-Silicon

Semiconductor selection involves a fundamental trade-off between X-ray stopping power (attenuation efficiency) and charge-carrier transport dynamics:

- Cadmium Telluride (CdTe) and Cadmium Zinc Telluride (CZT): Owing to the high atomic numbers of cadmium (Z=48) and tellurium (Z=52), CdTe/CZT sensors achieve >95% attenuation efficiency across the diagnostic energy spectrum (30-120 keV) with a compact crystal thickness of d = 1.4-2.0 mm.
- Silicon (Si): Silicon possesses a low atomic number (Z=14) and low attenuation density. A conventional face-on silicon detector would require an unmanageable crystal thickness (>30 mm) to stop diagnostic photons, severely increasing carrier transit times. To

overcome this, silicon PCD systems utilize an edge-on orientation, where X-rays enter parallel to the wafer surface, providing a long absorption path (30 mm) while keeping the charge collection distance (d≈ 0.5 mm) extremely short[7,9].

Carrier Drift, Diffusion, and Weighting Potential Localization

Under an applied electric field $E = V_b/d \approx 5$ kV/cm, generated electrons and holes drift toward their respective electrodes. Carrier drift velocity is $v_e = \mu_e.E$ and $v_h = \mu_e.E$.

In CdTe and CZT, electron mobility ($\mu_e \approx$ 1000-1100 cm²/V.s) is more than twenty times higher than hole mobility ($\mu_h \approx$ 50-80 cm²/V.s). Consequently, electron transit time across a 2 mm CdTe sensor is extremely fast:

$$t_{drift,\ e} = d/\ \mu_e.E\ \approx\ 30\text{-}50\ ns$$

where as hole transit time is prolonged ($t_{drift,\ h}$ ≈ 300-800 ns).

According to the Shockley-Ramo Theorem, the instantaneous current i(t) induced on a collecting pixel electrode by a moving charge q is determined by the velocity v(t) and the dimensionless weighting field $\vec{E}w(\vec{r}) = -\nabla\Psi_w(\vec{r})$:

$$i(t) = q\vec{v}(t).\ E_w(\vec{r})$$

In a classic planar parallel-plate detector, the weighting potential $\Psi_w(z) = z/d$ varies linearly with depth, causing the induced signal to depend heavily on interaction depth and slow hole drift.

PCDs prevent this depth dependence through the small-pixel effect. By designing pixelated anode electrodes with a pitch p much smaller than the sensor thickness d (aspect ratio p/d < 0.2, e.g., p = 0.15-0.3 mm, d = 2.0 mm), the weighting potential Ψ_w is near zero throughout almost the entire detector volume and rises sharply near the collecting anode surface.

As a result:

1. Signal induction occurs almost exclusively when electrons enter the immediate vicinity of the
anode (z/d > 0.8).
2. Slow hole drift toward the cathode induces negligible charge on the anode, eliminating ballistic deficit and tailing.
3. The induced current pulse becomes extremely fast, sharp, and electron-dominated, facilitating high count-rate performance.

During drift transit, thermal diffusion and Coulomb self-repulsion expand the initial charge cloud
laterally. The baseline diffusion spread $\sigma_\perp$ and Coulomb repulsion radius R_{Care}:

$$\sigma_\perp = \sqrt{2D_e t_{\text{drift}}} = d\sqrt{\frac{2k_B T_q}{V_b}} \approx 10 - 15\ \mu\text{m}$$

$$R_C = \left(\frac{3\mu_e Q_0 t_{\text{drift}}}{4\pi\epsilon_r\epsilon_0}\right)^{1/3} \approx 20 - 30\ \mu\text{m}$$

Combining these terms yields a total charge cloud diameter of 30-50 µm upon arrival at the anode plane.

Physical Non-Idealities and Signal Distortions

Despite direct conversion, PCDs encounter specific physical non-idealities that perturb the measured energy spectrum:

Charge Sharing

When an X-ray interaction occurs near the boundary between adjacent pixels, the expanding charge cloud (30-50 µm wide) is split across two or more pixel anodes. Consequently:

- Neither pixel receives the full charge Q_0; pulse heights in both pixels are reduced, causing counts to migrate into lower energy bins.
- If shared signals exceed threshold T_0 in multiple pixels, a single incident photon is falsely registered as multiple lower-energy counts (double counting).

The probability of charge sharing P_{share} scales with the effective perimeter-to-area ratio of the pixel:

$$P_share \approx 1 - \left(1 - \frac{2\,\alpha\,\ell_{eff}}{p}\right)^2 \approx \frac{4\,\alpha\,\ell_{eff}}{p}$$

where l_{eff} is the effective charge cloud radius and p is pixel pitch. As pixel size p shrinks to improve spatial resolution, charge sharing increases sharply[7,9].

K-Shell Fluorescence Escape

In CdTe and CZT sensors, photoelectric absorption in cadmium (K-edge = 26.7 keV) or tellurium (K-edge = 31.8 keV) prompts the emission of characteristic K-fluorescence X-rays (23-27 keV).

Because fluorescence photons have a mean free path of 60-100 μm in CdTe, they frequently escape the primary interaction pixel:

- Primary Pixel Signal: Deposited energy is reduced to $E_{primary} = E_{incident} - E_{Fluoro}$, creating a distinct K-escape peak in the measured spectrum[1,7].
- Secondary Pixel Signal: The escaped fluorescence photon is absorbed in a neighboring pixel, generating a false secondary count at E_{Fluoro}.

Pulse Pileup and Dead Time Limitations

Diagnostic CT subjects detectors to ultra-high photon flux levels exceeding 10^9 photons/s/mm². When two or more photons hit the same pixel within the finite shaping time τ_s of the front-end ASIC, their induced voltage pulses overlap—a phenomenon known as pulse pileup.

Pulse pileup causes two severe distortions:

1. Peak Pileup (Energy Distortion): Overlapping pulses sum together, forming a single artificial pulse whose amplitude exceeds the higher threshold T_k. Photons are counted in falsely elevated energy bins.
2. 2. Tail Pileup (Count Loss & Saturation): High arrival rates prevent the baseline from recovering, holding the signal above threshold and causing subsequent events to be missed.

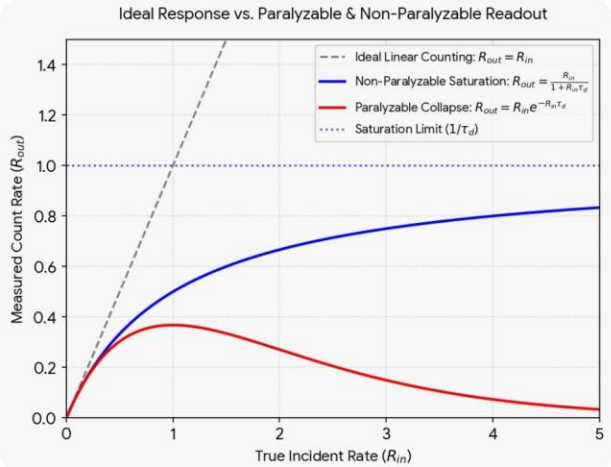
Readout electronics exhibit either paralyzable or non-paralyzable dead-time behavior. In a non paralyzable system, the measured count rate R_{out} relates to true incident rate R_{in} and dead time τ_d via:

$$R_{out} = \frac{Rin}{1+Rin\,.\,\tau d}$$

In a paralyzable system, subsequent events during dead time extend the insensitive period, yielding:

$$R_{out} = R_{in} \cdot e^{-R_{in}\tau_d}$$

Under extreme flux, paralyzable detectors experience throughput collapse, where R_out drops toward zero[7,10].



Front-End ASIC Architecture and Multi-Threshold Logic

To process femtocoulomb pulses at nanosecond timescales, each detector pixel is bonded directly to a

channel on a custom CMOS ASIC via solder bump-bonds[1].

The front-end processing pipeline consists of four sequential stages:

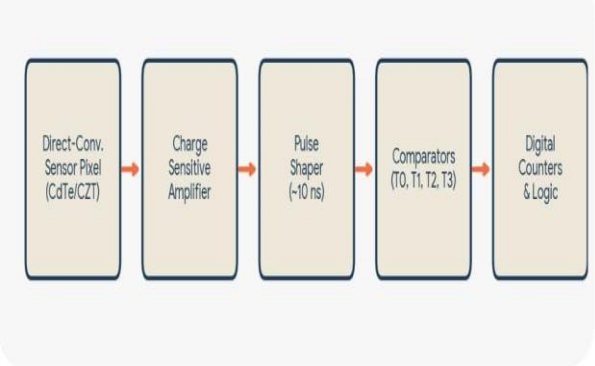
1. Charge-Sensitive Amplifier (CSA): Integrates the transient induced current i(t) from the sensor, converting charge Q_0 into a voltage step $V_{out} = Q_0 / C_f$, where C_f around 10-50 fF is the feedback capacitance. Continuous or switched feedback circuits restore the baseline[2].

2. Pulse Shaper: A bandpass filters low-frequency baseline fluctuations and high-frequency thermal noise. The resulting shaped pulse has a peak amplitude strictly proportional to E_{dep}[3].

3. Multi-Threshold Discriminators (Comparators): The shaped analog voltage pulse is fed simultaneously to a bank of high-speed comparators set to user-defined reference voltages V_{T0}, V_{T1},….., V_{TN}. Each comparator fires a digital pulse whenever the shaped waveform exceeds its voltage threshold.

4. Digital Counters and Anti-Coincidence Logic: Asynchronous digital counters increment upon rising-edge crossings. Energy bin data are generated by differencing counts between adjacent thresholds (e.g., Bin1 = Count(T_0) - Count(T_1)).

To correct charge sharing in real time, advanced ASICs (such as Medipix3, Timepix4, and Siemens Quantum technology) implement inter-pixel charge summing / anti-coincidence logic. When neighboring pixels trigger simultaneously within a tight coincidence window (approx 5-10 ns), hardware logic sums their analog pulse amplitudes, assigns the combined count to the pixel registering the highest individual signal, and inhibits false triggers in adjacent pixels.



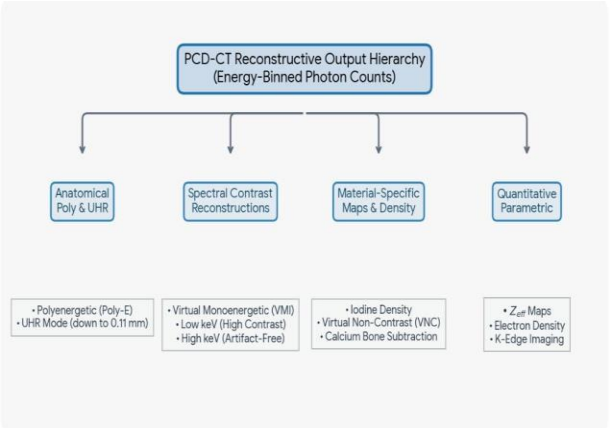
The mathematical mapping between the true incident photon energy spectrum S(E) and measured bin counts N_k is governed by the Spectral Response Function (SRF) matrix $M_{k,E}$:

$$N_k = \sum_m M_{k,E} S(E)$$

where $M_{k,E}$ = E[counts in Bin k] encapsulates charge creation statistics, transport loss, charge sharing, fluorescence escape, pulse pileup, and comparator threshold jitter into a unified matrix representation[7,10].

Reconstructive Outputs and Clinical Performance

The transformation from energy-binned photon counts to clinical images yields four major categories of diagnostic outputs:



Anatomical Reconstructions: Conventional- Polyenergetic and Ultra-High-Resolution (UHR)

- Polyenergetic Images: Energy-bin counts are weighted and summed to match the familiar contrast scale of conventional CT.
- Ultra-High-Resolution (UHR) Mode: Direct conversion enables physical pixel sizes down to 0.11-0.15 mm without septal dose penalties. Reconstructions using sharp kernels yield a spatial resolution of 16-17 lp/cm at the 10% Modulation Transfer Function (MTF) level (compared to 8- 9 lp/cm for standard EID-CT). This allows exquisite visualization of temporal bone ossicles, coronary stent struts, lung parenchymal reticulations, and subtle trabecular bone fractures[4,10,12].

Spectral Contrast Reconstructions:

Virtual Monoenergetic Imaging (VMI) VMI mathematically synthesizes images reflecting attenuation at a single monochromatic photon energy (keV):

- Low-keV VMI (40-50 keV): Exploits proximity to the iodine K-edge (33.2 keV), dramatically elevating iodine attenuation (HU) and boosting Contrast-to-Noise Ratio (CNR) by 40- 100%. This permits contrast medium volume reductions of up to 50\%, protecting patients with renal insufficiency.
- High-keV VMI (100-140 keV) Mitigates beam hardening, photon starvation, and metallic streak artifacts near orthopedic hardware, dental fillings, and vascular coils[5,6].

Material-Specific Maps

Using basis material decomposition (e.g., photo-electric/Compton or iodine/water basis functions), PCD CT isolates specific chemical constituents:

- Iodine Density Maps (mg/mL): Accurately quantifies local tissue iodine concentration, facilitating objective tumor vascularity grading and myocardial/pulmonary perfusion mapping.
- Virtual Non-Contrast (VNC) and Virtual Non-Calcium (VNCa): Subtracts iodine or calcium signals from contrast-enhanced scans, eliminating the need for unenhanced baseline scans and reducing total patient radiation dose[5,6,12].

Parametric Quantitative Reconstructions

- Effective Atomic Number (Z_{eff}) and Electron Density (ρ_e) Maps: Provides absolute elemental and physical density maps per voxel, aiding renal stone characterization (differentiating uric acid Z_{eff} ~ 7 from calcium oxalate Z_{eff} ~ 14 and providing precise stopping-power ratios for proton therapy planning.
- K-Edge Multi-Material Imaging: By positioning energy thresholds directly around the K-edge energy of targeted elements (e.g., Iodine at 33.2 keV, Gadolinium at 50.2 keV, Bismuth at 90.5 keV, or Gold nanoparticles at 80.7 keV), PCD-CT enables simultaneous, non-overlapping multi-contrast imaging within a single scan[5,6,8].

Table 2 synthesizes technical specifications and energy-threshold configurations across leading commercial and research PCD-CT platforms.

System / Manufacturer	Development Status	Sensor Material & Geometry	Energy Thresholds / Bins	Key Performance Characteristics & Features
NAEOTOM Alpha (Siemens Healthineers)	FDA-Cleared Commercial System	Cadmium Telluride (CdTe), Direct Conversion	4 Energy Bins (Configurable Thresholds, e.g., 20, 55, 70, 90 keV)	Dual-source design (2 X 144 slices), 0.11 mm native pixel pitch, 66 ms temporal resolution, UHR

				mode (17 lp/cm).
Photonova Spectra (GE HealthCare)	FDA-Cleared Commercial System	Deep-Silicon (Si) / CdTe Hybrid Architecture	Multi-threshold spectral binning	Edge-on deep silicon geometry, high count-rate stability, zero K escape artifacts in Si module.
CZT PCCT Prototype (Canon Medical / Redlen)	Clinical Research Prototype	Cadmium Zinc Telluride (CZT)	5 Configurable Energy Thresholds (e.g., 30, 51, 62, 72, 81 keV)	High atomic number stopping power, specialized anti-coincidence charge summing circuits.
MARS Spectral CT (MARS BioImaging)	Small-Animal / Extremity Platform	CdTe / CZT bonded to Medipix3RX ASIC	4-8 Energy Bins with Charge Summing	Spectroscopic micro-CT, real-time K-edge decomposition of gold, gadolinium, and iodine.

Discussion

Diagnostic Performance and Clinical Value

The clinical implementation of PCD-CT represents the most significant advance in computed tomography since the introduction of multi-detector helical scanning. By operating at the single-photon level and eliminating electronic noise, PCD-CT provides substantial quantitative and clinical benefits:

1. Radiation Dose Efficiency: Rejection of low-amplitude electronic noise allows diagnostic image quality to be maintained at ultra-low radiation doses. In pediatric, temporal bone, sinus, and lung screening protocols, radiation dose reductions of 80-85% have been demonstrated compared to standard EID-CT[1,4,12].

2. Standardization of "Always-On" Spectral Imaging: In dual-energy EID systems, spectral acquisition required deliberate pre-scan planning (e.g., dual-source switching, fast kV-switching, or dual-layer detectors). In PCD-CT, multi-threshold binning is intrinsically active for every routine scan. Radiologists can retrospectively generate low-keV VMI, iodine maps, or high-keV artifact reduction series on demand without additional radiation exposure.

3. Improved Small-Vessel and Stent Luminal Imaging: The combination of 0.11-0.15 mm pixel pitch and 16 lp/cm spatial resolution eliminates severe blooming artifacts from calcified coronary plaques and metallic stents, allowing accurate lumen stenosis grading previously impossible on EID CT[10,12].

Engineering Challenges and Technological Bottlenecks

While clinical results are impressive, semiconductor PCDs present complex engineering challenges:

1. Polarization under Extreme Flux: In CdTe and CZT detectors exposed to sustained high X-ray flux (> 10^8 photons/s/mm²), slow hole mobility leads to positive space-charge accumulation near the cathode. This internal space charge distorts the electric field, collapses carrier drift velocity, and shifts energy thresholds—a process known as polarization. Advanced contact engineering

(Schottky contacts), optimized bias voltages (1000 V), and doping adjustments are required to maintain temporal stability.

2. Dark Current Leakage: High bias voltages induce continuous dark-current leakage I_{dark} across sensor contacts. Fluctuations in I_{dark} load the CSA input, shift baseline voltages, and induce threshold drift, requiring continuous baseline-restoration circuitry on the ASIC[7,8].

3. ASIC Power Density and Thermal Management: High-density pulse-shaping circuits, comparators, and digital counters operating at hundreds of megahertz consume substantial electrical power (~ 0.9 mW/mm² or 90 mW/cm²). Cooling gantry-mounted detector arrays under tight space constraints requires sophisticated liquid or forced-air heat exchangers[7,8].

Future Outlook and Emerging Trajectories

The trajectory of PCD-CT development points toward several transformative innovations:

- Deep-Learning Spectral Reconstruction Pipelines: Machine-learning architectures (e.g., Physics Informed Neural Networks) are being integrated directly into projection-space material decomposition and image-space VMI synthesis. These models exploit spatial-spectral correlations to suppress image noise at 40 keV while preserving quantitative iodine accuracy.
- Theranostic and Targeted K-Edge Molecular Imaging: The ability to decompose multiple high-Z elements simultaneously enables novel molecular imaging protocols. Functional contrast agents (e.g., antibody-functionalized bismuth or gold nanoparticles) can target specific tumor receptors or inflammatory plaques while iodinated contrast outlines vascular anatomy in a single scan.
- Cross-Platform Standardization and Calibration: As multiple vendors release PCD-CT systems with distinct sensor materials (CdTe, CZT, Si) and threshold logic, international physics organizations (AAPM, ICRU) are establishing standardized calibration phantom protocols to ensure HU and iodine concentration (mg/mL) comparability across platforms[5,6,8].

Conclusions

Photon-counting detector CT represents a profound technological leap in medical X-ray imaging[1,2]. By converting individual X-ray interactions directly into electron-hole pairs and evaluating pulse heights through multi-threshold front-end ASICs, PCD-CT rejects electronic noise, eliminates optical septal dead zones, and preserves photon energy information[1,7]. Despite physical challenges such as charge sharing, K escape, and pulse pileup, advanced ASIC charge-summing logic and spectral correction algorithms enable routine ultra-high spatial resolution (16-17 lp/cm), dose reductions up to 85%, and quantitative spectral material decomposition. PCD-CT establishes a new gold standard for diagnostic radiology, bridging microscopic physical signal formation with advanced clinical diagnosis[2,7,12].

References

1. Flohr T, Petersilka M, Henning A, Ulzheimer S, Ferda J, Schmidt B. Photon-counting CT review. *Phys Med.* 2020;79:126-136. doi:10.1016/j.ejmp.2020.10.030
2. Willemink MJ, Persson M, Pourmorteza A, Pelc NJ, Fleischmann D. Photon-counting CT: Technical principles and clinical prospects. *Radiology.* 2018;289(2):293-312. doi:10.1148/radiol.2018172656
3. Kreisler B. Photon counting detectors: Concept, technical challenges, and clinical outlook. *Eur J Radiol.* 2022;149:110229. doi:10.1016/j.ejrad.2022.110229
4. McCollough CH, Rajendran K, Leng S, et al. The technical development of photon

counting detector CT. *Eur Radiol.* 2023;33(8):5321-5330. doi:10.1007/s00330-023-09545-9

5. Schwartz FR, Sodickson AD, Pickhardt PJ, Sahani DV, Lev MH, Gupta R. Photon-Counting CT: Technology, current and potential future clinical applications, and overview of approved systems and those in various stages of research and development. *Radiology*. 2025;314(3):e240662. doi:10.1148/radiol.240662
6. Perera Molligoda Arachchige AS, Darvizeh F. Understanding photon-counting CT: Physics, detector technology, and image reconstructions. *Sensors.* 2026;26(17):5574. doi:10.3390/s26175574
7. Chen GH, Lai R, Li K. A physics primer on photon-counting detectors in CT: Physics, signal formation, and performance. *Med Phys.* 2026;53(2):e70586. doi:10.1002/mp.70586
8. Hsieh SS, Leng S, Rajendran K, Tao S, McCollough CH. Photon counting CT: Clinical applications and future developments. *IEEE Trans Radiat Plasma Med Sci.* 2021;5(4):441-452. doi:10.1109/TRPMS.2020.3007380
9. Sharma S, Ravin CE, Samei E. A framework to model charge sharing and pulse pileup for virtual imaging trials of photon-counting CT. *Phys Med Biol.* 2024;69(22):10.1088/1361-6560/ad8b0a
10. Taguchi K, Iwanczyk JS. Vision 20/20: Single photon counting x-ray detectors in medical imaging. *Med Phys.* 2013;40(10):100901. doi:10.1118/1.4820371
11. Leng S, Bruesewitz M, Tao S, et al. Photon-counting detector CT: System design and clinical applications of an emerging technology. *RadioGraphics.* 2019;39(3):729-743. doi:10.1148/rg.2019180115
12. Rajendran K, Petersilka M, Henning A, et al. First clinical photon-counting detector CT system: Technical evaluation. *Radiology*. 2022;303(1):130-138. doi:10.1148/radiol.212579